



Provided by the author(s) and University of Galway in accordance with publisher policies. Please cite the published version when available.

Title	Finite element simulation of fretting wear and fatigue in thin steel wires
Author(s)	Leen, Sean B.
Publication Date	2013-05-09
Publication Information	Cruzado, A., Leen, S. B., Urchegui, M. A., & Gómez, X. (2013). Finite element simulation of fretting wear and fatigue in thin steel wires. <i>International Journal of Fatigue</i> , 55, 7-21.
Publisher	Elsevier ScienceDirect
Link to publisher's version	http://dx.doi.org/10.1016/j.ijfatigue.2013.04.025
Item record	http://hdl.handle.net/10379/5411
DOI	http://dx.doi.org/10.1016/j.ijfatigue.2013.04.025

Downloaded 2024-03-13T08:02:28Z

Some rights reserved. For more information, please see the item record link above.



Accepted Manuscript

Finite element simulation of fretting wear and fatigue in thin steel wires

A. Cruzado, S.B. Leen, M.A. Urchegui, X. Gómez

PII: S0142-1123(13)00131-X

DOI: <http://dx.doi.org/10.1016/j.ijfatigue.2013.04.025>

Reference: IJF 3118

To appear in: *International Journal of Fatigue*

Received Date: 28 November 2012

Revised Date: 12 April 2013

Accepted Date: 28 April 2013



Please cite this article as: Cruzado, A., Leen, S.B., Urchegui, M.A., Gómez, X., Finite element simulation of fretting wear and fatigue in thin steel wires, *International Journal of Fatigue* (2013), doi: <http://dx.doi.org/10.1016/j.ijfatigue.2013.04.025>

This is a PDF file of an unedited manuscript that has been accepted for publication. As a service to our customers we are providing this early version of the manuscript. The manuscript will undergo copyediting, typesetting, and review of the resulting proof before it is published in its final form. Please note that during the production process errors may be discovered which could affect the content, and all legal disclaimers that apply to the journal pertain.

Finite element simulation of fretting wear and fatigue in thin steel wires

A.Cruzado^{1*}, S. B. Leen², M.A.Urchequi³, X.Gómez¹

¹*Mondragon Goi Eskola Politeknikoa, Mondragon Unibertsitatea, Loramendi 4, 20500 Arrasate-Mondragon (Spain)*

²*Mechanical and Biomedical Engineering, National University of Ireland Galway, Ireland*

³*ORONA eic, Polígono Industrial Lastaola s/n, 20120 Hernani (Spain)*

Corresponding author:

E-mail:acruzado@mondragon.edu

Fax number: +34 943 79 15 36

Telephone number: +34 943 25 33 63

Abstract

This paper studies the effect of fretting on fatigue life reduction of thin steel wires, using the frictionally-induced multiaxial contact stresses obtained from a finite element wear model, validated in previous work. The fatigue life prediction model uses a critical-plane SWT approach in a 3D crossed cylinder problem. A new damage accumulation methodology for the adaptive mesh simulation, based on the cyclic material removal, has been developed. Four methods (Manson's universal slope, Muralidharan modified universal slopes, Medians and fatigue S-N curves) for the estimation the fatigue coefficients of the wire have been used. Manson's method and medians method give lives closer to those obtained from fretting wear tests in thin steel wires. The other methods are more conservative. The methodology predicts correctly the life reduction of this components due to the increase of the normal load (contact pressure), while it is not clearly predicted that an increase of the stroke reduces the life of these components as shown in the experimental testing. Guidelines for developing a more robust methodology are proposed.

Keywords: Fretting wear, Wire ropes, Crack nucleation, Finite elements, Wear simulation

MOMENCLATURE

b	Fatigue strength exponent
c	Fatigue ductility exponent
d_n	Damage of the current cycle in the surface layer n equal to $w_{k+1,n}$
d'_n	Interpolated damage from the previous cycle to the current cycle in the surface layer n
D_n	Damage of the first cycle equal to $w_{1,n}$ & Accumulated damage in the current cycle in the surface layer n
$\Delta\epsilon_a$	Normal strain amplitude
Δn	Incremental wear depth
Δn	Cycle jump
x	Stroke
E	Young's elastic modulus
ϵ'_f	Fatigue ductility coefficient
f	Coefficient of friction
F_f	Friction force
F_n	Normal Load
f_r	Frequency
k	Volumetric coefficient of wear
k_l	Local wear coefficient
n	layer number
n	Number of cycles
N_i	Number of cycles to crack initiation
$N_{i,l}$	Number of cycles to failure in each element for each FE fretting cycle l
N_f	Predicted number of cycles to failure
p	Local contact pressure
p_{av}	Mean contact pressure
p_{max}	Maximum contact pressure
R_a	Surface average roughness
s	Relative slip
σ_{ij}	ij components of local stress tensor
σ'_f	Fatigue ductility coefficient
σ_{max}	Maximum normal stress on the critical plane
σ_u	Ultimate strength
σ_y	Yield strength
t	Time
T	Temperature
w	Miner's damage criterion
W_v	Volumetric wear
x,y,z	Cartesian coordinates
y_n	y coordinate of the current cycle
Y_n	y coordinate of the first cycle & y coordinate of the Accumulated damage

1 Introduction

Wire ropes combine two very useful properties: high axial strength and flexibility in bending. These properties convert wire ropes into indispensable load transmission elements for many industrial applications. For instance, wire ropes are widely used in cranes, mine hoisting, and lifts. These mechanical properties of the ropes are largely dependent on their construction and the properties of the wires itself, because the wires are wound into strands, which are then wound around a central core to form the wire rope, as shown in Fig. 1. The properties of the rope depend on the number, size and arrangement of the wires in the strands, the number and arrangement of the strands and the core type.

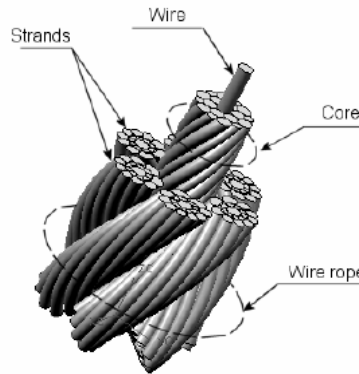


Fig. 1. Schematic of a wire rope composed of different strands of wound steel wires.

Nevertheless, when the ropes run over the sheaves the wires are subjected to the combine axial tensile load and bending stretch load, which leads to an oscillatory motion between the neighbouring contacting wires. This phenomenon results in a fretting wear damage mechanism as reported by Schrems [1] and Waterhouse [2]. More recently, Urchegui et al. [3] studied this effect into a 7x19 stranded rope, where the fretting problem is presented in point contacts, typically between the outermost wires of strands and core or between the outermost wires of adjacent strands. As a consequence of fretting wear in point contacts, different failure modes could be presented: catastrophic rupture of the wire due to the considerable reduction of the resistant area produced by the wear, fatigue life reduction due to the stress concentration factor produced by the wear scar and the fretting induced fatigue cracks which leads in the rupture of the thin steel wire. In this work it is proposed to study the effect of wear-induced evolution of sub-surfaces stresses in the fretting induced fatigue crack initiation.

In the literature different studies about the fatigue life prediction of steel wires have been reported. LLorca and Sánchez-Gálvez [4] presented a model to determine the fatigue limit and the fatigue life to explain the results obtained experimentally in 7 mm diameter wires. This study takes into account that the fatigue fracture initiates in all cases at a surface flaw and neglect the crack initiation. Beretta and Boniardi [5] proposed a suitable method for fatigue

strength prediction and quality control of wires which consist of: tensile tests for estimating fatigue threshold of long cracks ($\Delta K_{th,lc}$), cyclic tensile tests for evaluating the theoretical fatigue limit, determination of the extreme value of sampling and fatigue strength prediction using El-Haddad model. In this study wires of 1 and 0.9 mm diameter were used. Petit et al. [6] presented a study of fatigue crack propagation in 0.95 mm steel wires. Lambrighs et al. [7] showed the influence of the inclusion parameters, such as the inclusion size, location, composition and geometry on the fatigue properties in a 0.175 mm and 0.3 mm diameter wires. Navaei et al. [8] used three damage models to predict the fatigue life of 1 mm diameter wires: linear damage rule (LDR), damage curve approach (DCA) and Double linear damage rule (DLDR). After comparing with experimental results the DCA approach is presented as the best method for patented steel wires. Brighenti et al. [9] analysed the effect of the residual stresses on fatigue behaviour of a notched wire with surface crack subjected to alternating tension, showing that the crack propagation phenomenon is accelerated by increasing residual stresses. These studies mainly show that the fatigue crack initiates from inner or surface defects presented in the steel wires. Nevertheless in the case of wire rope systems, as has been mentioned previously, the cracks initiate inside the wear scars, as a consequence of the stress concentration factor or as a consequence of the fretting induced multiaxial stresses. Zhang et al. [10] studied the effect of fretting wear scars in 1mm diameter wire obtained from 90° crossing cylinders arrangements fretting tests that subsequently were subjected to a fatigue tests. It was observed that the rupture of the wire was located in the deepest point of the wear scar, demonstrating that the fatigue life was inversely proportional to the fretting wear depth. The main reason of this effect is the stress concentration at this point and the following crack initiation, propagation and fracture of fretted wire. Following these tests and including fretting wear scars for different crossing angles, Wang et al. [11] proposed an equation to investigate the effect of fretting wear on fatigue fracture properties of steel wires assuming that the fretted scar (fretting wear depth) on the wire surface was the initial pre-crack. To this end the Paris equation and an equation which represent the evolution of dimensionless stress intensity factor crack growth in pure tension was proposed. The dimensionless stress intensity factor was obtained from the assumption that the crack assumes a semicircular shape from very early and tends to flatten. Recently, in order to analyse the effect of fretting-fatigue in 1mm diameter wire, Wang et al. [12] have proposed a new fretting fatigue test rig for steel wires. All the tests were performed under mixed fretting regime conditions. It was concluded that an increase of displacement amplitude at each cyclic strain level increases the tangential force and the relative slip range at the stabilized stage, accelerating the fretting damage of the contact surface. Based on this experimental configuration Wang et al. [13] performed a numerical FE analysis employing the multiaxial fatigue criteria of Fatemi-Socie and Smith Watson-Topper to analyse the effect of fretting parameters on the crack initiation location in the initial fretting fatigue

stage in both partial sliding and gross sliding conditions. This study showed that the crack initiation is more likely to occur in the trailing edges of the contact. Furthermore it was reported that the crack initiation becomes more difficult with increasing the contact load and decreasing the stroke. Nevertheless it has not been proposed any methodology for predicting both the fretting crack location and the crack initiation life in steel wires being one of the key factors in this analysis the material removal. Because the effect of wear in some cases such as in gross sliding conditions could be positive to remove the cracks and lengthen the fatigue life, or in other cases such as in partial sliding conditions or mixed fretting regimes, could be negative to change the contact conditions and produce the crack initiation.

In the recent years many researchers have introduced the multiaxial fatigue models to establish life predictions in fretting problems. Szolwinski and Farris [14] were the first researchers that introduced the critical plane methods with the Smith-Watson-Topper (SWT) parameter to predict fretting fatigue life from fretting induced stresses. Araujo and Nowel [15] demonstrated that the SWT and the Fatemi-Socie (FS) multiaxial fatigue models combined with analytical approach such as Mushkelishvili potential theory to determine the two dimensional contact stress field in cylinder on flat configurations, resulted in overly conservative predictions at smaller contacts due to the presence of high stress gradients. So they proposed two averaging methods, which combined with the multiaxial fatigue criteria, resulted in a less conservative prediction. Fouvry et al. [16] also used an averaged stress approach, due to the very sharp stress gradient imposed below the surface in a cylinder on plane configuration. It was proposed the introduction of a representative damage volume with the Crossland's multiaxial fatigue criterion for predicting the crack nucleation under stabilized partial slip conditions.

Sum et al. [17] developed a finite element based implementation of the critical plane SWT fatigue life method. It was shown that this methodology captures the well known contact size effect of the cylinder plane configuration shown previously by Araujo and Nowel [15]. Madge et al. [18] proposed a finite element based method to predict and characterise the role of fretting wear on fretting fatigue for a rounded punch-on-flat Ti-6Al-4V under partial slip and gross sliding conditions. This model combined a finite element wear simulation model with the critical plane SWT fatigue model. They concluded that the prediction of fretting wear was a critical aspect for predicting fretting fatigue, which can not be predicted by models that do not include the effects of material removal. Recently Zhang et al. [19] used a similar model in a round of flat and round punch on flat configuration for the wear evolution and crack nucleation predictions. It was concluded that if the modelling of wear was not taken into account the fatigue damage prediction could be under-conservative in the partial slip regime (PSR) and over conservative in the gross slip regime (GSR).

Based on the different studies reported in the literature, firstly the analysis of the fatigue life prediction for wire ropes requires investigations of the wear contact problem originated changes

in the contact region, because the reciprocal sliding between the wires, which generates considerable wear, can modify the wire shapes in contact permanently, both during tension and bending of the rope, that implies the continuum change of the subsurface stresses. Secondly in order to acquire a better understanding of the fatigue behaviour of ropes, the severe fatigue degradations that occur between contacting wires has to be implemented using multiaxial fatigue models.

In a previous works [20] the influence of fretting wear in 0.45 mm diameter thin steel wires under different loading conditions was analysed. In these tests, it was detected that under high normal loads and strokes cracks initiate at a certain number of cycles. More recently with the aim to predict fretting wear scars and reduce the time consuming and the associated cost that requires the experimental data, and optimized FE wear simulation approach for thin steel wires was developed and validated [21], based on the fretting wear tests carried out in the previous work.

As a consequence of the extremely complex inner stress range appeared in this type of components, due to the complex structure and behaviour shown by the wire rope systems, the present paper is the first step to develop a FE tool for predicting fretting induced cracks in wire rope systems. In this work it is proposed to study the fretting wear caused fatigue life reduction of the wires, using the frictionally induced multiaxial contact stresses obtained from a FEM wear model developed previously. To this end the multiaxial critical plane SWT approach with a new damage accumulative model, which takes into account the material removal in the accumulated damage, has been developed. The results obtained from this tool have been compared with the experimental data obtained from fretting wear tests of thin steel wires, giving in the end guidelines for the construction a more robust tool in future works.

2 Experimental details

2.1 Material

The wires used for the experiments are wires which are usually fabricated into a 7x19 rope (7 strands with 19 individual wires in each one) as presented in Fig. 1. For the tests, wires with a diameter of 0.45 mm, were used. They are cold-drawn from eutectoid carbon steel with 0.8% C with a hardness of 659 ± 81 HV0.05. The tensile properties obtained from the measured stress-strain curve shown in Fig. 2, were an ultimate strength of 3000 MPa and an offset 0.2% yield strength of 2688. The surface average roughness (R_a) of these wires along its axis was 0.35 and 0.70 μm in perpendicular direction. These values were obtained from the measurements carried out at an unworn wire using a confocal imaging profiler (Plu, Sensofar). The tensile properties and the Vickers hardness are summarized in Table 1.

	E (GPa)	σ_u (MPa)	σ_y (MPa)	% RA	HV 0.05
Wire	200	3000	2688	33	659±81

Table 1. Mechanical properties of the 0.45 mm diameter wire.

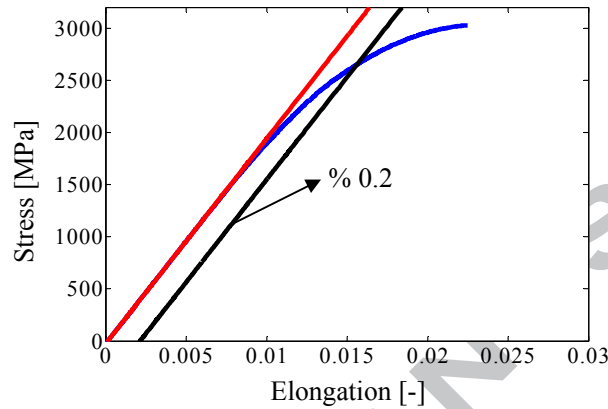


Fig. 2. Experimentally obtained engineering stress-strain curve for 0.45 mm diameter wire.

2.2 Tribological testing

An extended description of the experimental testing and results used to study the fretting induced cracks in thin steel wires is reported in [20]. In this section it is briefly outlined the test rig and the conditions that were selected for the analysis of the subsurface stresses and the crack initiation life prediction using the FE damage approach proposed in this paper.

Fretting wear tests between thin steel wires were carried out on specific tribometer for small sliding amplitudes (10 - 200 μm) and small loads (0.1 - 10 N). The tribometer consists of a top arm with an integrated load cell for the measurement of the friction force and a bottom vibrating horizontal table. The movement of this table is given by a frequency-controlled DC motor with an eccentric adjustment. Special holders were designed for the correct fixing of the wires. In these holders the wires represent a toroid with a curvature radius of 10mm. The bottom holder is fixed to the vibrating horizontal table in the tribometer, with the wire axis parallel to the direction of motion. The upper holder (stationary sample), is fixed at the end of a horizontal arm forming the desired crossing angle between its axis and the bottom wire axis. During each test the real stroke (Δx_{real}), friction force (F_f) and total linear wear (W_{tot}) were measured. Relative humidity (RH) and temperature (T) were kept constant during the test. All measured quantities were recorded on-line multiple times. After each test the frictional and wear quantities used in the FE wear model were obtained.

The tests were carried out with 90° crossing angle configuration in a range of mean contact pressures that goes from 2460 MPa to 3933 MPa, two strokes 65 μm and 130 μm in a range of cycles that ranges from 20000 to 200000. The specific details of these tests are shown in Table 2. After the tests the contact surfaces were analysed by optical microscopy in order to find crack and no crack conditions. Only fretting cracks were found in the bottom specimen, so the FE analysis will be focused on this specimen.

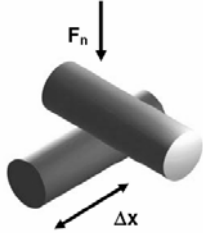
PARAMETER	SYMBOL	VALUE	TRIBOSYSTEM
Normal Load (N)	F_n	1, 2, 3, 4	
Mean contact pressure (MPa)	p_m	2460; 3100; 3600; 3933	
Maximum contact pressure (MPa)	p_{\max}	3690; 4650; 5400; 5900	
Stroke (μm)	x	65 \pm 5 (2N, 3N, 4 N) / 130 \pm 5 (1N, 2N)	
Frequency (Hz)	f_r	10	
Number of cycles (10^3)	N	20; 50; 100; 200	
Lubricant		None	
Temperature ($^{\circ}\text{C}$)	T	25 \pm 1	
Relative humidity (%)	RH	50 \pm 5	

Table 2. Fretting test conditions for the study of crack initiation process in 90° crossed cylinders steel wires.

3 FEM Methodology

3.1 FE model

The FE model used in this study is the same that has been validated in a previous work [21], for the simulation fretting wear in thin steel wires under different loads conditions. The model consists of two cylinders with a diameter of 0.45mm contacting together at 90° crossing angle as shown in Fig.3. Moreover the curvature radius that acquires the wire in the fixation support (10 mm) is included.

The load and the boundary conditions are applied in the free surfaces of the model through a surface-based coupling, which couples the motion of all free surfaces to the motion of a reference node. Moreover a kinematic coupling is used, so as the rigid body motion is defined by the reference node. It allows in the upper wire, where a normal force is applied in the reference point, only the vertical movement and in the bottom wire, where an alternative displacement condition is imposed, only the horizontal movement. This is because the wire maintains the rigid body movement of the holder in the testing machine. The elastic isotropic material model was specified in both cylinders, in which a standard values for steel (Young's modulus of 210 GPa and Poisson's ratio of 0.33) have been used. Although in this study contact

pressures greater than the yield strength of the material which produce plastic deformation were used, it was not define an elastic plastic model. On the one hand plastic deformations only are given in the first cycles. Because the wear produces a rapidly increase of the contact area which leads into a drastically decrease of the contact pressure, being negligible the effect of the plastic deformation along the fretting tests. On the other hand the introduction of an elastic plastic model produces convergence problems in the contact resolution and increases the computational time.

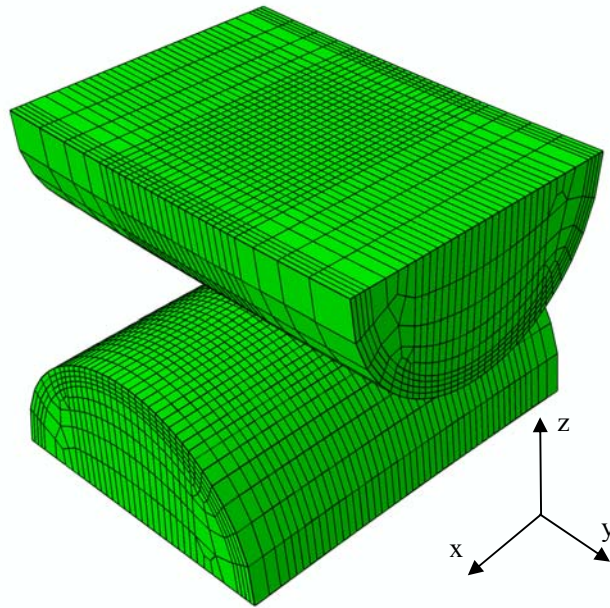


Fig. 3. FE model and mesh details of the 90° crossed cylinder fretting wear test.

The meshes are carried out according to a partition methodology, in which a more refine mesh is used in the contact zone, to capture precisely the variation of contact pressures and geometry. The mesh is composed of square shape eight nodes lineal brick elements. The size of the meshes in the contact zone is defined following the optimized mesh criterion to reduce the computational time proposed for fretting wear scars modelling [21]. Taking into account that, an optimum mesh should be in the range from 3% to 4% of the final longitudinal wear width and that the dimensions of the wear scars analysed in this study are in the range from 250 μm to 310 μm , a 10 μm x 10 μm x 7.5 μm mesh size which corresponds to the 4% of the smallest wear scar dimension is chosen. As reported in [21] smaller mesh sizes only increase the computational time without any improvement in the final result and greater mesh sizes only give a poor discretization of the wear scar.

The contact surface interaction between both cylinders is defined via the finite sliding contact pair algorithm, which uses the master–slave algorithm to enforce the contact constraints. In this study the top surface is chosen as slave surface and the bottom one as master. The Lagrange multiplier contact algorithm was used to ensure the exact stick constrain when the shear stress is less than the critical value according to the Coulomb friction law. A coefficient of friction f of 0.7 is chosen according to the experimental tests carried out in thin steel wires.

3.2 Wear modelling

The specific method used in this study for the wear simulation of thin steel wires, which was validated satisfactorily under different range of loads and slip amplitudes, is described in detail in the work reported by Cruzado et al. [21]. The wear model used for the fretting wear simulation is the Archard's modified equation proposed by McColl et al. [22]. This equation assumes that fretting wear can be evaluated by applying Archard's equation to local contact conditions along the entire contact interface. The wear local model is described by the Eq. 1:

$$\Delta h(x,t) = k_l \cdot p(x,t) \cdot s(x,t) \quad (1)$$

where $\Delta h(x,t)$, $p(x,t)$ and $s(x,t)$ are the incremental wear depth, the contact pressure and the relative slip for a specific point x (node) at specific time t , respectively. On the other hand k_l represents the local wear coefficient. This coefficient in principle could not be the same as the volumetric coefficient of wear k , because the last one represents an average value across the complete wear scar. Nevertheless some authors like McColl et al. [22] or Fouvry et al. [23] have justified the close relation existed between the local wear coefficient k_l and the volumetric coefficient of wear k . In this work the volumetric coefficients of wear k corresponding to each specimen and test conditions, which are shown in table 3, have been used. It has to be pointed out that the wear simulations presented in this study will be carried till 50000 number of cycles.

	<i>Coefficient of wear k ($10^{-8} \text{ mm}^3/\text{Nmm}$)</i>		<i>Coefficient of wear k ($10^{-8} \text{ mm}^3/\text{Nmm}$)</i>	
	<i>Top-Bottom</i>		<i>Top-Bottom</i>	
2N-65 μm -50000 cycles	2.11 – 1.57	1N-130 μm -50000 cycles	2.32 – 2.34	
3N-65 μm -50000 cycles	2.10 – 1.91	2N-130 μm -50000 cycles	2.32 – 2.34	
4N-65 μm -50000 cycles	2.32 – 2.34			

Table 3. Coefficients of wear obtained from fretting wear tests under different loads-stroke conditions.

Taking into account Eq. 1, one fretting cycle is divided in small slip increments; it implies that the FE wear simulation is the product between these increments and the total number of cycles. As a consequence, high computational time is needed for the simulation of one fretting test. In this point the cycle jump technique proposed by different authors like McColl et al. [22] and Mary et al. [24] is used, where it is made the assumption that the contact pressure and the slip distribution remain constant in each finite element analysis over the next Δn cycles. In this way Eq. 1 is multiplied by Δn to obtain Eq. 2, such that the wear corresponding to Δn cycles can be simulated in one FE fretting cycle. In the study carried out by Cruzado et al. [21] was reported that an optimum simulation without any distortions in profile should be carried out with 100 fretting FE cycles, 40 increments/fretting FE cycle and the corresponding Δn . Where the Δn is obtained dividing the desired number of cycles n by the 100 fretting FE cycles that compose one FE simulation, e.g. for 50000 number of cycles a Δn of 500 is used.

$$\Delta h(x, t) = \Delta n \cdot k_l \cdot p(x, t) \cdot s(x, t) \quad (2)$$

The implementation of the wear model has been carried out using the ABAQUS user subroutine UMESHMOTION [25], in which the spatial adjustment of the contact nodes is done within an adaptive framework. Nevertheless this subroutine only gives the contact results for one of the contacting surfaces (slave surface), i.e., so the transition of the contact pressures and slips from the slave surface to the master surface is done according to the nearest interpolation method, since this method is presented computationally the most efficient [21].

3.3 Damage modelling

Fretting wear in thin steel wires leads to produce a frictionally induced multiaxial contact stress distribution, which is in constant changing due to the wear induced evolution of the subsurface stress. This condition with the combination of high loads and strokes leads to produce fatigue cracks in the contact surface. Moreover during these tests, the fretting induced multiaxial stress field is combined with the high tensile stress produced as a consequence of the bending that suffers the wire in the fixation holder. The greater influence of the tensile stresses, as will be discussed in section 4.2 leads to produce fracture mode I cracks.

With the purpose to study the multiaxial fatigue phenomenon presented in thin steel wires, the critical plane Smith-Watson-Topper (SWT) multiaxial fatigue criterion, generally used in cases involving tensile cracking, has been implemented. This criterion has been applied satisfactorily by many researchers for the prediction the crack nucleation life and location in fretting problems, both in fretting fatigue loading conditions [14, 15, 17, 26] and in fretting wear loading conditions [19, 27, 28]. The SWT parameter predicts that the crack initiation and growth occurs on a certain plain, where the normal stress and strain in that plane is maximum.

The parameter is shown in Eq. 3, where σ_{\max} is the maximum normal stress in the critical plane and $\Delta\epsilon_a$ is the normal strain amplitude in the same plane, E is the Young modulus, σ'_f and b are the Basquin strength coefficients corresponding to the high cycle fatigue (HCF), ϵ'_f and c are the Coffin-Manson fatigue ductile coefficients corresponding to low cycle fatigue (LCF) and N_i represents the number of cycles needed for the crack initiation.

$$SWT = \sigma_{\max} \cdot \Delta\epsilon_a = \frac{\sigma_f'^2}{E} (2N_i)^{2b} + \sigma_f' \epsilon_f' (2N_i)^{b+c} \quad (3)$$

The implementation of this method in the FE model presented previously has been carried out according to the methodology proposed by Sum et al. [17] and Das and Sivakumar [29] for 3D problems. This methodology consists of the three-dimensional transformation (Mohr's circle) of the stress and strains of each element centroid at intervals of 5° over 180° , analyzing all the planes that can be found in a semi-sphere. So in each centroid are recorded 1296 planes for each element and for each increment that form one fretting cycle. From this data the maximum normal stress σ_{\max} and the normal strain amplitude $\Delta\epsilon_a$ are recorded in each plane of each element, where $\Delta\epsilon_a$ represents the difference between the maximum and the minimum value of strain normal to the candidate plane over the entire fretting cycle. Finally the SWT values are obtained for each candidate plane and each element, which are then used to obtain the maximum SWT value in the critical plane of each element. With the maximum SWT value and solving Eq. 3, the numbers of cycles to failure for each fretting cycle are obtained.

Nevertheless, due to the material removal effect, the stresses and strain are changing from cycle to cycle. To capture this phenomenon the general Eq. 3 is used to predict the number of cycles to failure $N_{i,l}$ in each element for each FE fretting cycle l , where the damage corresponding to each FE fretting cycle l is accumulated using the Miner-Palmgren linear fatigue accumulation damage rule shown in eq. 4. Thus the crack nucleation is occurred when the total accumulated damage w in a material point reaches 1. In this study, as the wear simulation problem is computationally costly, a cycle jump technique was used for the wear modelling optimization. Therefore, the damage accumulation model is expressed as Eq. (4), where $N_{i,l}$ is the critical-plane SWT predicted number of cycles for crack initiation at fretting FE cycle l , n is the desired number of cycles simulated in the FE fretting wear model and Δn is the cycle jump value. The ratio between n and Δn represents the 100 fretting FE cycles of which one FE simulation is composed, as mentioned in section 3.2.

$$w = \sum_{l=1}^{\frac{n}{\Delta n}} \frac{\Delta n}{N_{i,l}} \quad (4)$$

On the other hand, as a consequence of the adaptive meshing used in the FE wear simulation approach to update the mesh due to the material removal, the damage can not be accumulated in the same centroidal point from cycle to cycle. The reason is because the centroidal position of each element is changing from cycle to cycle, so the damage accumulated in the centroid position of a previous wear cycle could not be the same in the new centroidal position of the current cycle. The previously accumulated damage in this point should be less, such as the damage goes decreasing from the surface to the inner of the material. So the effect of material removal in the damage eradication has to be considered.

To solve this problem Madge et al. [18] proposed to create a material point mesh (MPM) as the global reference model for damage accumulation. In this method the nodes of the MPM have fixed coordinates through the analysis, so the cyclic damage calculated at the centroid of each element was linearly interpolated back to the MPM for accumulation, and the nodes corresponding to the removed material don't accumulate any fatigue damage.

In this study, due to the high amount of wear produced by the fretted thin steel wires a new damage accumulation model based on the previous and on the current location position of the element centroid due to wear has been developed. This approach leads to update the damage in the new centroidal position after the FE wear simulation cycle. The mesh used for the wear modelling in the adaptive meshing framework is shown in Fig 4. Taking into account that the crack initiation is produced close to the surface layers and due to the great amount of data that is collected in a 3D problem, only the third first layers of the centroid points will be used in this new methodology.

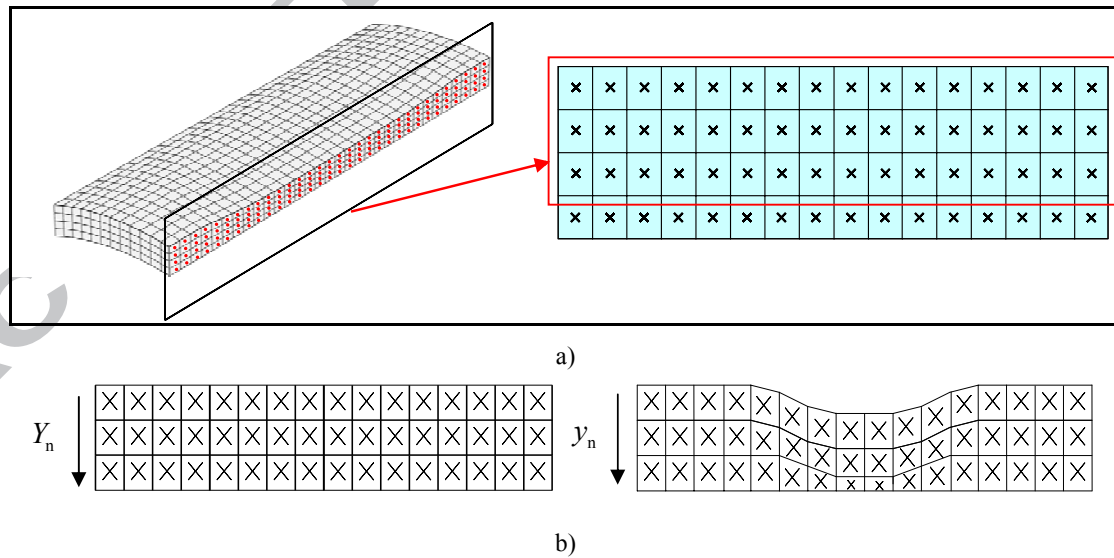


Fig. 4. FE mesh in the adaptive meshing framework and each centroid points: a) 3D FE mesh with a cut of one of the longitudinal plans, b) FE mesh with the centroid points before and after the wear process.

A flowchart which summarises the proposed process for determining the accumulation of damage due to the wear removal is shown in Fig. 5.

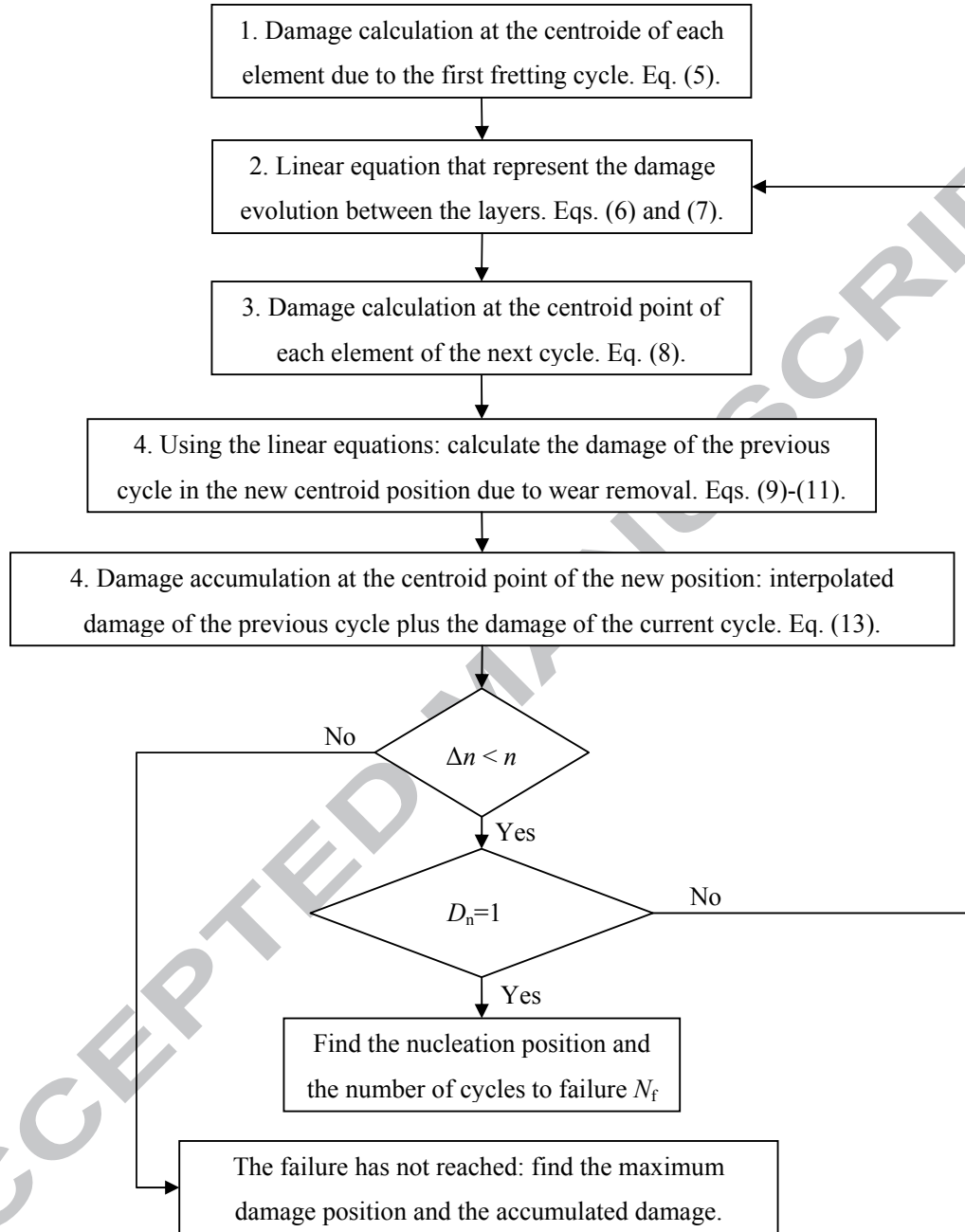


Fig. 5. Flow chart of the accumulative damage model due to the effect of the material removal.

So the following methodology for the application the accumulative damage rule due to wear is outlined here:

1. Cyclic damage D_n due to the first fretting cycle is calculated at the centroid point location Y_n of each element in the first three layers n (Fig.4b left). D_n is calculated according to Eq. 5, where Δn is the cycle jump value and $N_{i,1,n}$ is the critical-plane SWT predicted number of cycles for crack initiation at the first fretting FE cycle of each element in the first three layers n .

$$D_n = w_{1,n} = \frac{\Delta n}{N_{i,1,n}} \quad (5)$$

2. As a consequence of the material removal, the damage obtained in the centroidal points Y_n of the first cycle will not be maintained in the new centroidal position location y_n reached after the second cycle due to wear (Fig.4b right): so two linear equations as shown in Eqs. (6) and (7), which represent the damage evolution between the first and the second layer and the second and the third layer, are constructed. The graphic representation is shown in Fig. 6a.

$$D_1(Y) = \frac{D_2 - D_1}{Y_2 - Y_1} (Y - Y_1) + D_1 \quad (6)$$

$$D_2(Y) = \frac{D_3 - D_2}{Y_3 - Y_2} (Y - Y_2) + D_2 \quad (7)$$

3. Cyclic damage d_n due to the second fretting cycle is calculated at the new centroid point location y_n of each element in the first three layers as it is shown in Fig. 6b. d_n is calculated according to Eq. 8, where Δn is the cycle jump value and $N_{i,l+1,n}$ is the critical-plane SWT predicted number of cycles for crack initiation at the second fretting FE cycle of each element in the first three layers n .

$$d_n = w_{l+1,n} = \frac{\Delta n}{N_{i,l+1,n}} \quad (8)$$

4. The damage of the first fretting cycle is interpolated back to the new position at the centroidal point's location y_n of the second cycle, as presented in Eqs. (9-11) and in Fig. 6c.

$$d'_1 = \frac{D_2 - D_1}{Y_2 - Y_1} (y_1 - Y_1) + D_1 \quad (9)$$

$$d'_2 = \frac{D_3 - D_2}{Y_3 - Y_2} (y_2 - Y_2) + D_2 \quad (10)$$

$$d'_3 = \frac{D_3 - D_2}{Y_3 - Y_2} (y_3 - Y_2) + D_2 \quad (11)$$

5. In the new centroid position (Eq. (12)) of each element, as it is shown in Fig. 6d, the interpolated damage d'_n due to the first cycle is accumulated with the damage of the second cycle d_n (Eq. (13)).

$$Y_n = y_n \quad (12)$$

$$D_n = d_n + d'_n \quad (13)$$

6. Two new linear equations (Eqs. (6) and (7)) are constructed for the new centroid position due to wear (Eq. (12)), and the new damage values (Eq. (13)), as represented in Fig 6d.
7. This process is repeated as many times as number of cycles needed to reach the damage failure, when Eq. (13) reaches 1.

In order to reduce the postprocessing time required by this damage accumulation process, and knowing that the relocation of the new centroidal position in the third layer after each wear and remeshing cycle is very small, an extrapolation of the third layer damage using the equation corresponding to the second and third layer Eq. (7) was carried out as shown in Fig.6 c. Therefore, taking into account that $Y_3 \approx y_3$ the error committed in the damage reduction calculation of the previous cycle in the current cycle is very small. This error will be accumulated from cycle to cycle in the construction of the new linear equation of both layers Eqs. (6) and (7); nevertheless as the damage of the second and third layer is very small comparing with the damage of the first layer, this error is negligible.

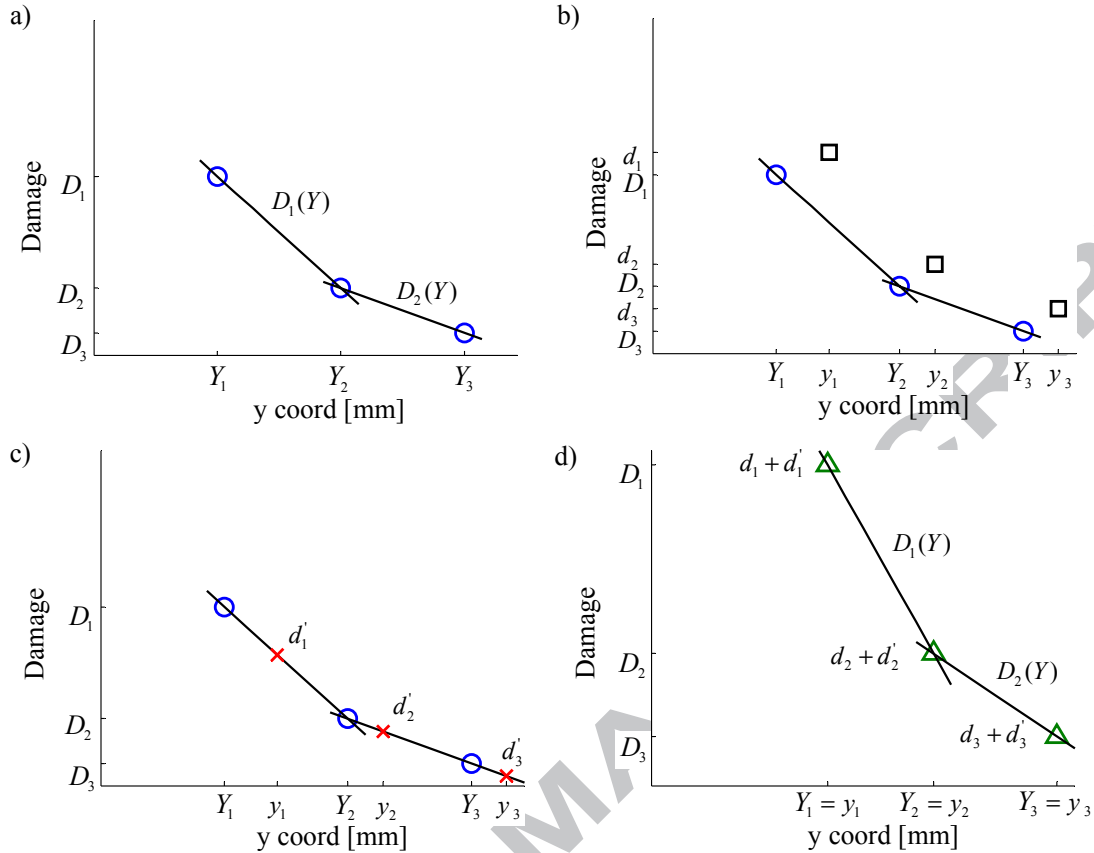


Fig. 6. Damage accumulation process: a) Damage of the first cycle (circle) in the first three layers and the two linear equations which represent the evolution of the damage between the layers, b) damage in the second FE cycle due to wear (square), c) damage of the first cycle interpolated back to the new centroid position of the second cycle (x), d) accumulated damage in the second cycle (triangle) and the new linear equations (graphic b (square) plus graphic c (x)).

3.4 Material fatigue constants

In the absence of fatigue properties of the wire studied in this work, different approaches, for obtaining the fatigue strength coefficients and the fatigue ductility coefficients needed for the life prediction according to the SWT model (Eq. (3)), are discussed in this section.

The first approach is based on the methods proposed by different authors for estimating the fatigue coefficients based only on the available monotonic tensile test data. This methodology has been used previously by Del Llano-Vizcaya et al. [30] for predicting the fatigue lives in helical compression springs which are made by high carbon steel wires, using different multiaxial fatigue criteria. In table 4 are shown the different estimation methods proposed in this study. The first one corresponds to the Manson's universal slope method [31], which takes into account the ultimate strength of the material σ_u and the true fracture strain ϵ_f which is calculated using the reduction in area RA $\epsilon_f = \ln(1/(1-(RA/100)))$. The second one is a

modified universal slopes method proposed by Muralidharan and Manson [32], in which both fatigue exponents are increased and the σ_u/E term is introduced for the calculation of both fatigue coefficients. The last method named Medians method for steel is introduced by Meggiolaro and Castro [33], which combines good average life predictions with one of the lowest standard deviations for a higher range of different steels.

<i>Parameter</i>	<i>Universal Slopes</i>	<i>Modified universal slopes</i>	<i>Medians (steels)</i>
σ'_f	1.9 σ_u	$0.623 \sigma_u^{0.823} E^{0.168}$	1.5 σ_u
b	-0.12	-0.09	-0.09
ϵ'_f	$0.76 \epsilon_f^{0.6}$	$0.0196 \epsilon_f^{0.6} (\sigma_u/E)^{-0.53}$	0.45
c	-0.6	-0.56	-0.59

Table 4. Estimation methods of fatigue coefficients from monotonic tensile tests. [31-33]

The second approach is based on obtaining the fatigue properties from an eutectoid high strength steel wire reported in the literature. So, the Basquin's (HCF) coefficients were obtained from the R=0.1 uniaxial fatigue tests reported by Beretta and Mateazzi [34] in a 1.97 mm diameter wire with an interlamellar spacing of about 0.1 μm . The mechanical properties of this wire are shown in Table 5 and are in accordance with those ones reported by Verpoest et al. [35] for 1.99 mm diameter wire. To obtain the σ'_f and b in fully alternated tension-compression fatigue tests R=-1 the standard Goodman relationship was used to correct the mean stress effect. In the absence of low cycle strain controlled fatigue data, ϵ'_f and c were obtained applying the monotonic tensile stress properties in the Manson's universal slope method presented previously.

A summary of the fatigue coefficients obtained from the monotonic tensile test properties of the studied steel wire shown in Table 1 and for the different methods proposed in Table 4 are shown in Table 6. Moreover in this table are included the fatigue coefficients obtained from the S-N curves reported by Beretta and Mateazzi [34] in a 1.97 mm diameter wire.

	σ_u (MPa)	σ_y (MPa)	% RA	%E	HV
Beretta	1855	1540	58	1.61	470±30

Table 5. Mechanical properties of Beretta's 1.97 mm diameter wire. [34]

<i>Parameter</i>	<i>Universal Slopes</i>	<i>Modified universal slopes</i>	<i>Medians (steels)</i>	<i>Beretta</i>
σ'_f	5700	3521	4500	8000
b	-0.12	-0.09	-0.09	-0.225
ϵ'_f	0.441	0.1053	0.45	0.697
c	-0.6	-0.56	-0.59	-0.6

Table 6. A summary of the fatigue coefficients obtained from the different methods.

4 Results and discussions

The FE analysis presented in this section corresponds to the fretting wear tests carried out on a 0.45mm diameter pre-stressed wire, as a consequence of the bending that was applied in the wire for the correct fixation in the holder. With the aim to analyse the fretting wear frictionally induced crack nucleation, firstly a study of the subsurface stress distribution in a not pre-stressed steel wire has been carried out. Secondly the effect of the bending imposed pre-stresses in the fretting induced subsurface stresses has been analysed. Thirdly the results obtained from combined FE wear model and the critical plane SWT and damage approach proposed in this paper has been discussed and compared with the results obtained experimentally. Finally different strategies for the improvement the developed methodology for predicting fretting wear cracks in thin steel wires have been proposed.

4.1 Subsurface stress distribution analysis

The wear-induced material removal evolution of sub-surfaces stresses which directly controls the crack initiation in the bottom cylinder after different number of cycles and 1N-130 μ m is discussed in the following paragraphs. A three dimensional local axis coordinate system with the local 1 direction parallel to the direction of the movement (x direction in Fig. 3); the local 3 direction normal to the contact surface (z direction in Fig. 3), and the local 2 direction making a right hand set with the other two has been used. The sub-surface stresses have been plotted in the local 1 direction parallel to the direction of the movement, in the central path $y=0$ of the contact at a depth of 3.5 μ m, which corresponds to the first row of centroidal values of the lower specimen. This path matches with the maximum SWT location that will be presented in section 4.3. Furthermore all subsurface stresses plotted in this paper are belonging to the left hand side motion of the lower wire. It means that the contact area is moving to the right hand side and thus the sliding between the upper (static) and the lower wires is produced in this direction. At the mirror, these figures represent the opposite direction motion of the lower wire.

In Fig. 7 the σ_{11} and σ_{13} stresses value after 20000 number of fretting wear cycles and different displacement amplitude locations are shown. It can be seen from these plots that there is an increase of the peak stress value from the centre position to the end position of the

displacement amplitude, being its greater value in this last position. This is because of the shape acquired by the wear scar, composed by a uniform surface geometry that goes from the centre to the near edge of the wear scar and with inclined flanks in edge the wear scar.

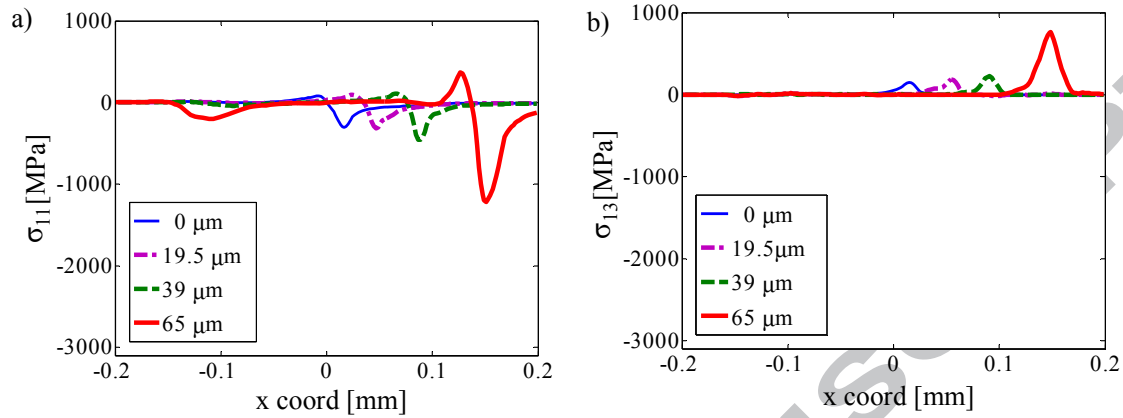


Fig. 7. Subsurface stress distribution for 1N-130 μ m, 20000 number of cycles and different amplitude displacement locations: a) stress distribution σ_{11} , b) stress distribution σ_{13} .

Fig. 8 shows the multiaxial subsurface stress distribution for different number of cycles at a displacement amplitude position of 65 μ m which corresponds to the maximum stresses peak value presented in Fig. 7. It can be seen that there is a drastic reduction in the peak stress value before and after wear, as a consequence of the decrease at the peak contact pressure in the first few hundred of cycles as reported in [21]. On the other hand, while a tensile stress parallel to the surface promotes a crack nucleation a compressive traction retards it. Taking into account this affirmation, the σ_{11} axial stress in the direction of sliding and the σ_{13} shear stress are the key components in the crack nucleation process, as σ_{22} mainly presents compressive stresses and σ_{12} is the shear stress appeared in the transversal direction to the movement, located in the x coord of the maximum σ_{11} and σ_{13} value. The value of the σ_{12} in the longitudinal path is 0 MPa. Moreover while σ_{13} is only governed by tensile stresses, σ_{11} is governed by both states. It can be seen in Fig. 7a that while the leading edge of the contact (the front side in the sliding direction) is subjected to compressive stresses, the trailing edge of the contact (the back side in the sliding direction) is subjected to a tensile stresses. Furthermore, due to the increase of the length of the wear scar, a translation of the peak stresses in the sliding direction is produced. This effect is smaller as the number of cycles increase.

When analyzing the values of the tensile stresses in σ_{11} , σ_{13} and σ_{12} (σ_{22} is not considered because only gives compressive stresses), it can be derived that the shear stress, which corresponds to the shear stress in the sliding direction, is the most critical. This tendency is

maintained along the number of cycles. As an example it can be seen that while for 50000 numbers of cycles $\sigma_{13} = 455\text{MPa}$, $\sigma_{11} = 181\text{MPa}$ and $\sigma_{12} = 100\text{MPa}$.

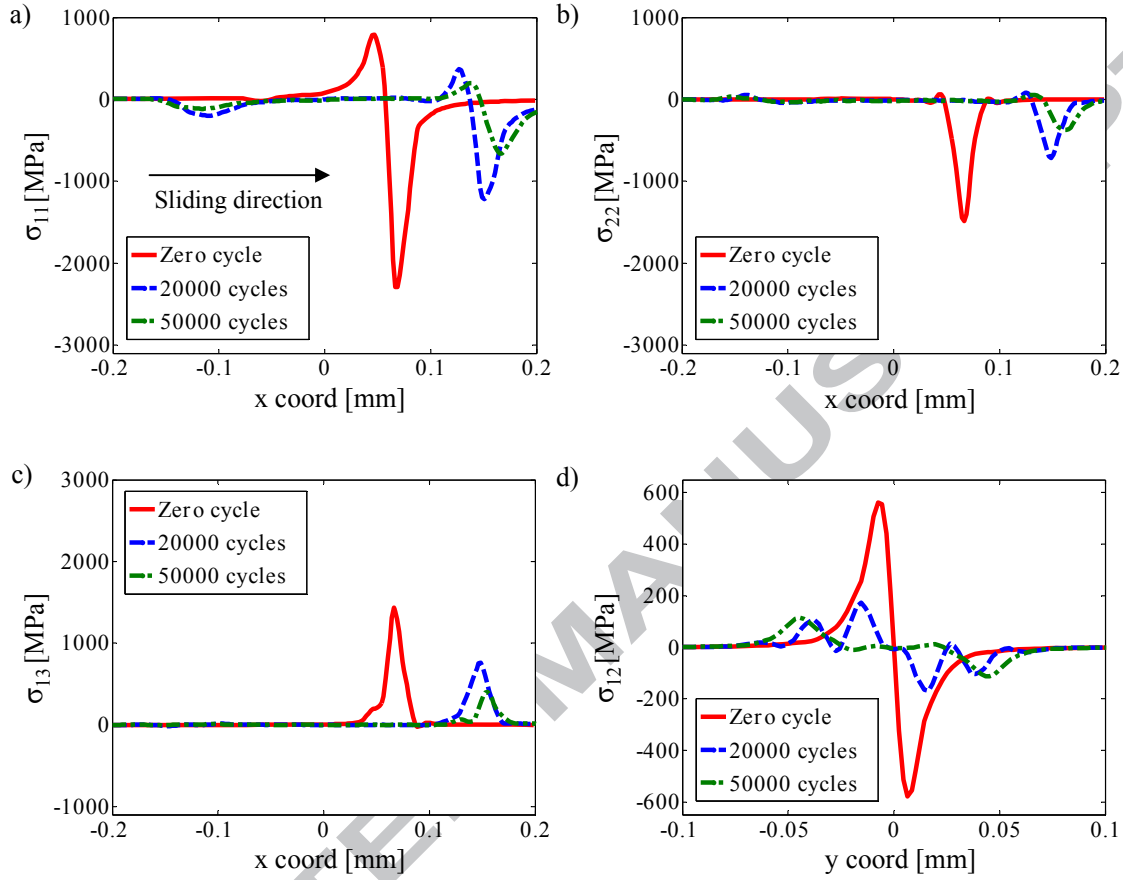


Fig. 8. Multiaxial subsurface stress distribution in the bottom cylinder for 1N-130 μm and different number of cycles in the amplitude displacement position of 65 μm : a) stress distribution σ_{11} , b) stress distribution σ_{22} , c) shear stress distribution σ_{13} and c) shear stress distribution σ_{12} .

The effect of the coefficient of friction in the previously shown key components in the crack nucleation, the axial stress σ_{11} and the shear stress σ_{13} for 1N-130 μm before wear is illustrated in Fig.9. The σ_{22} and the σ_{12} are not plotted in this study, because these components present the smallest influence in the crack initiation as has been shown previously and the coefficient of friction has low influence in this two stresses. In this study these components are governed by the contacting load, such as σ_{22} represent the compressive stress and σ_{12} the shear stress produced by the normal load. If a rotation or a tensional moment in the x axis was introduced, σ_{12} would have greater influence.

A reduction of the coefficient of friction implies a reduction of the subsurface tensile stresses in both the axial stress σ_{11} and the shear stress σ_{13} . It means that reducing the coefficient of friction, it could be increase the crack nucleation life. As has been mentioned in section 3.1, in this study a friction coefficient of 0.7, which is in accordance with the coefficient of friction obtained experimentally in the stable period [20] has been used.

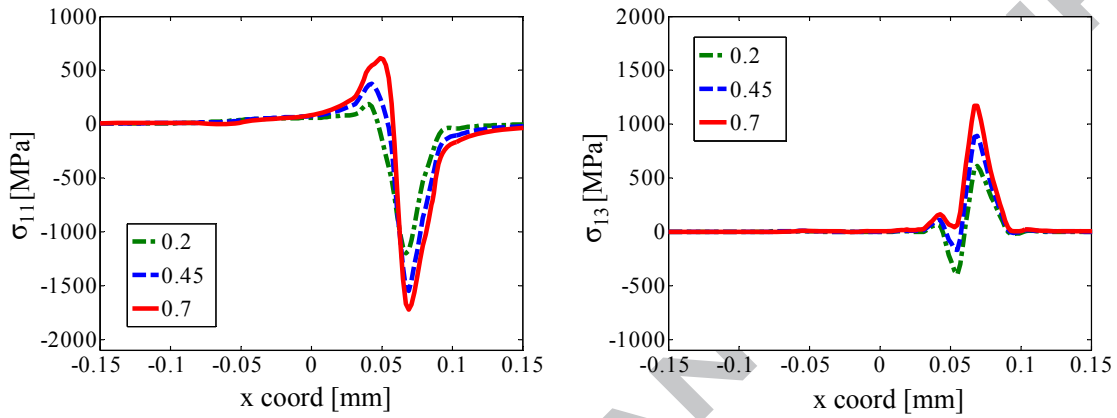


Fig. 9. The axial subsurface distribution for 1N-130μm and different coefficient of friction: a) stress distribution σ_{11} , b) shear stress distribution σ_{13} .

4.2 Subsurface stress distribution in a pre-stressed wire

In the previous paragraphs the analysis of the fretting induced subsurface multiaxial stress distribution has been described. Nevertheless, the curvature used to correctly fix the wire in the holder, produces a bending deformation in the wire which leads to introduce tensile stresses near the contact surface.

To analyse the stress field produced in the wire as a consequence of the bending, in Fig. 10 it is shown the FE model used for modelling the wire fixation procedure in the holder. While the wire supporting holder and the two fixation washer have been modelled as a 3D analytical rigid body, the wire has been modelled according to an elastic plastic model with isotropic hardening. The elastic plastic model has been introduced using the measured stress-strain curve shown in Fig. 2. The mesh is composed of eight nodes lineal brick elements. The contact surface interactions between the rigid surfaces and the wire are defined via the finite sliding contact pair algorithm. With the aim to simplify the problem no frictional contact has been considered.

Fig. 10 shows the stress produced in the axial direction of the wire σ_{11} which is in accordance with the axis coordinate system defined in the previous section. This stress, in combination with fretting induced multiaxial stresses, will affect in the crack nucleation process. It can be seen that in the region corresponding to the contact surface in fretting tests, it is produced a

compressive stress in the bottom side of the wire and a tensile stress in the top side of the wire which corresponds to the contact surface. The results show that there is a tensile stress $\sigma_{11} \approx 2000\text{MPa}$ near the contact surface. On the other hand the stresses σ_{22} and σ_{33} in the contact region are less than 5% of the stress obtained in σ_{11} , so they will be neglected in the study of the combined fretting and bending produced bulk stress study.

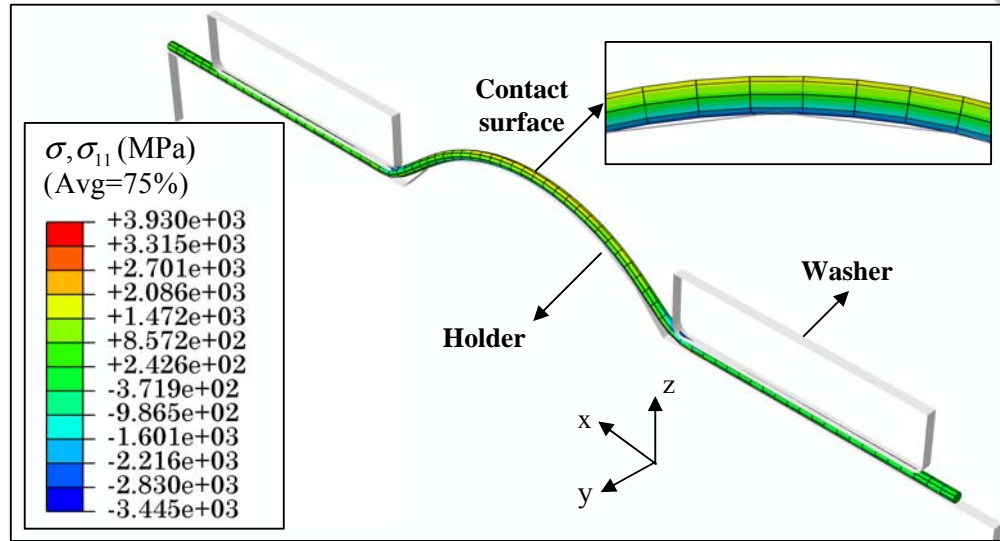


Fig. 10. Elastic-plastic finite element analysis of the wire fixation σ_{11} (MPa) axial stresses.

To analyse the effect of the pre-stresses in the fretting wear analysis, an initial predefined state, obtained after applying a tensile pressure of 2000MPa in the extremes of the wire, has been introduced in the bottom cylinder of the fretting wear model. Fig. 11 shows the axial stress σ_{11} and the shear stress σ_{13} for 1N-130 μm and 50000 number of cycles, with and without pre-stresses. The σ_{22} and σ_{12} stresses are not considered in this analysis because the tensile stress introduced as a consequence of the bending has not influence in this two stresses.

The effect of the pre-stress is significant in the σ_{11} axial stress, where an increase of the tensile stresses along the entire contact region is shown. Moreover it can be seen a decrease of the tensile stresses in the front side of the contact as a consequence of the compressive stresses produced by the leading edge of the contact, as has been discussed previously. On the other hand the σ_{13} shear stress presents a less significant increase in the tensile stresses. It suggests that a decrease of the wire pre-stresses, e.g. increasing the bending radius, it can be increase the crack nucleation life. Moreover it can be derived that while in a non pre-stressed wire the shear stress σ_{13} is the most critical, in the pre-stressed wire the tensile traction σ_{11} becomes the most critical value in the crack initiation, leading fracture cracks in mode I.

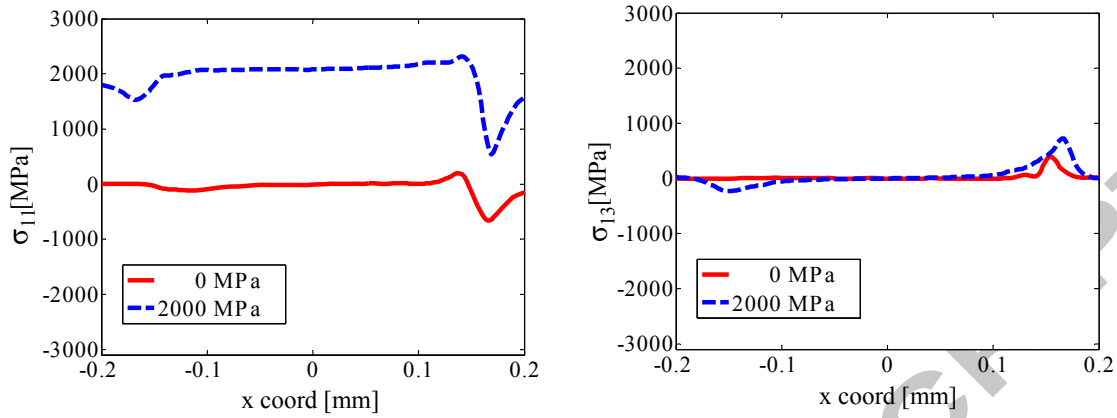


Fig. 11. The axial subsurface stress distribution for 1N-130 μ m, 50000 number of cycles and different pre-stresses in the amplitude displacement position of 65 μ m: a) stress distribution σ_{11} , b) shear stress distribution σ_{13} .

4.3 Fatigue crack nucleation analysis

Firstly, the analysis of the crack nucleation prediction due to fretting wear in thin steel wires has been carried out according to the proposed FE methodology. Secondly, the results have been compared with the experimental data obtained from fretting wear tests.

Fig.12 illustrates the critical plane SWT crack nucleation predictions plots for the case of 1N-130 μ m pre-stressed wire at 2000 MPa. Fig.12a shows the maximum SWT critical plane value along the axial direction of the bottom wire (sliding direction). The results show that there is a drastic decrease of the SWT peak value (Fig. 12b) in the first thousand of cycles and then, this value stabilizes and decreases at a lower slope. This effect is attributed to the material removal produced by the wear, which causes stress redistribution as shown previously due to the increase of the contact area that promotes a decrease of the contact pressure. While the maximum SWT value is distributed along the entire contact surface in a fretting cycle in which there is no wear, as the wear occurs a peak value appears in the edge of the contact. Moreover as a consequence of the wear and the widening of the wear scar this peak value suffers and outward movement, the same tendency presented previously with the axial stress σ_{11} and the shear stress σ_{13} .

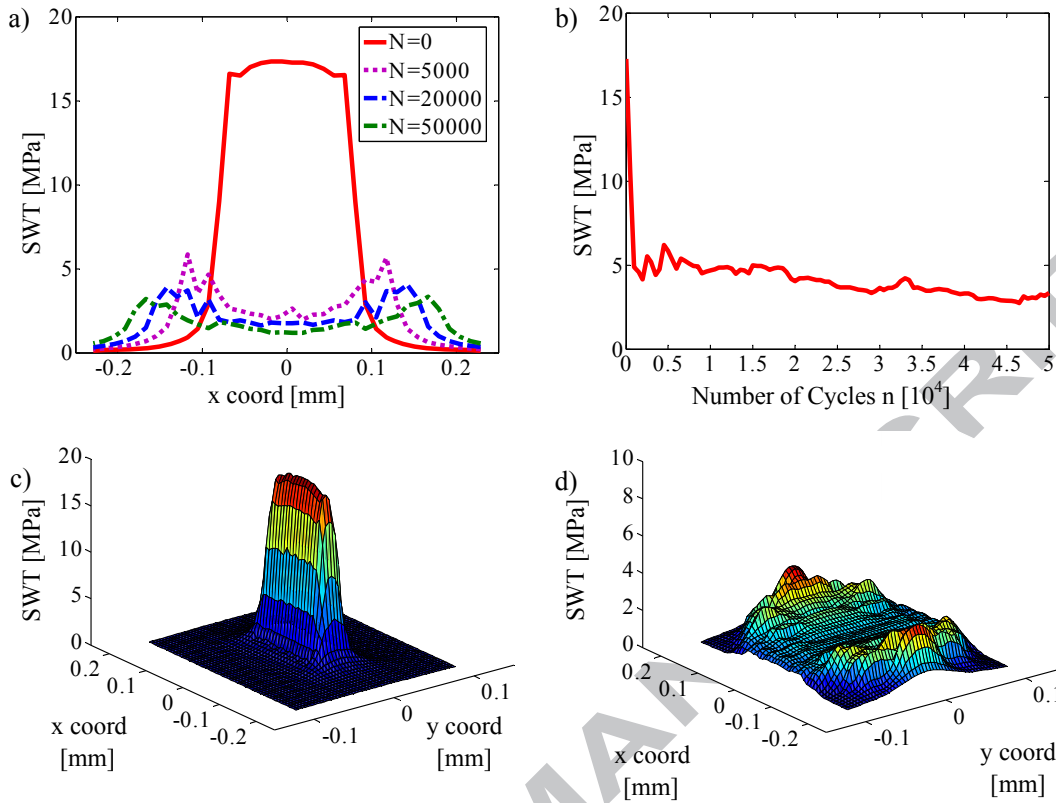


Fig. 12. FE critical plane SWT plots for 1N-130 μ m and 2000 MPa pre-stress: a) longitudinal SWT value plot for different number of cycles, b) evolution of SWT peak value, c) 3D plot of the SWT value without wear, d) 3D SWT value plot after 50000 number of cycles.

On the other hand the 3D SWT contour plots are shown in Fig. 12c for the no wear case and in figure Fig. 12d after 50000 fretting wear cycles. As the wear is produced it can be seen the two symmetrical SWT peaks in both edges of the axial direction. This peak value start in the middle of the transversal direction of the wear scar and goes decreasing outside this position. Furthermore from both graphics, the no wear case and the wear case, it is obtained that the path corresponding to the maximum SWT critical plane value along the direction of the movement, is located in the central path $y=0$.

Fig. 13 shows the effect of the bending induced pre-stresses in the SWT peak value. In both cases the pre-stressed and the not pre-stressed wire, the tendency is the same, there is a decrease of the maximum peak value in the first thousand of cycles and then stabilised. Nevertheless, the influence of the tensile stresses produced as a consequence of the bending leads to a drastic increase in the peak value, which could reduce considerably the fretting induced crack initiation life. Furthermore in Fig. 13b is shown that the location of the maximum SWT peak value in the axial direction after 50000 numbers of cycles, in both cases is in the edge of the contact, being this distance from the centre of the wear scar a little bit higher in the pre-stressed case than in

the not pre-stressed case. So reducing the bending of the wire it can be increase drastically the life of this component.

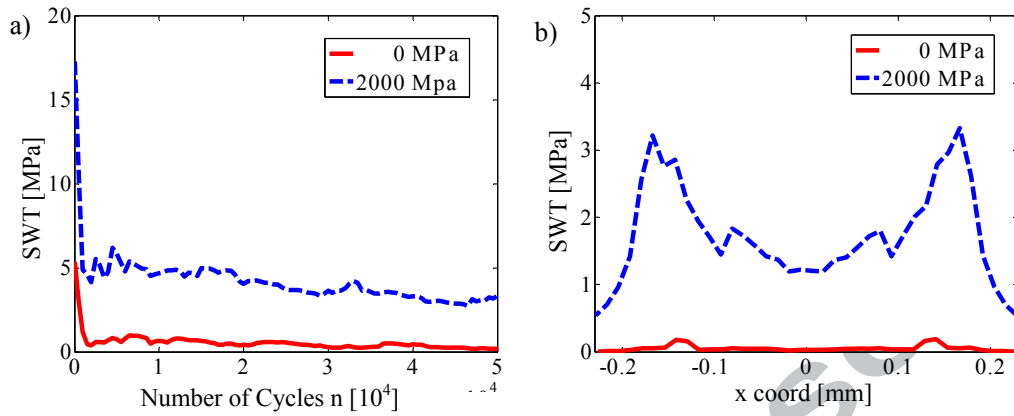


Fig. 13. FE critical plane SWT plots for 1N-130 μ m with and without pre-stress: a) SWT peak value evolution, b) longitudinal plot of the maximum SWT value.

Fig. 14 shows the crack initiation locations of the bottom wear scars after carrying out fretting wear tests with 4N-65 μ m (Fig. 14a) and 2N-130 μ m (Fig. 14b) and 20000 cycles. Two symmetrical transversal cracks at a specific distance from the centre of the wear scar are produced. This is in accordance with the SWT critical plane plots presented previously in Fig. 13b. On the other hand the crack propagation is produced in the longitudinal plane to the contact surface, as a consequence of the fiber structure presented by the wire. This is because during the cold drawn process the pearlitic structure of the eutectoid steel is formed by lamellas of cementite and ferrite oriented in the longitudinal direction of the wire. The wear scars obtained with the FE wear simulation model, for the two cracks experimental cases presented previously are shown in Fig. 15. The good correlation of this methodology is shown in the dimensions of the wear scars.

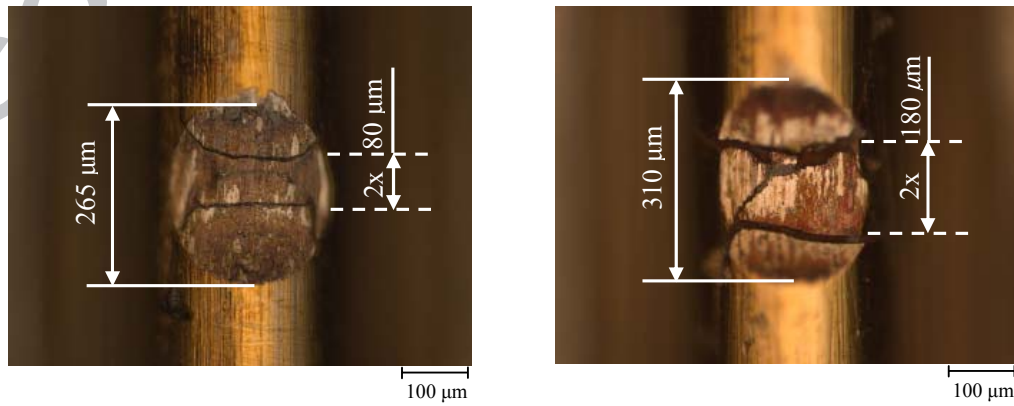


Fig. 14. Failure of the wire under different conditions fretting wear tests: a) 4 N-65 μ m-2 $\times 10^4$, b) 2 N-130 μ m-2 $\times 10^4$.

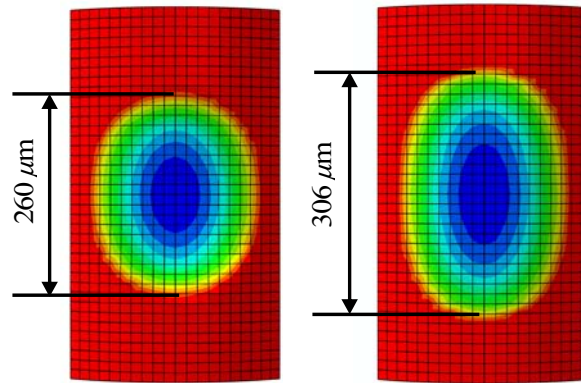


Fig. 15. FEM simulated wear scars for: a) 4 N-65 μm - 2×10^4 , b) 2 N-130 μm - 2×10^4 .

The life predictions made combining the SWT critical plane approach and the damage accumulation model, which takes into account the continuum evolution of the subsurface stresses due to wear removal are summarised in Table 7. The life predictions have been carried out according to the fatigue coefficients obtained from the three methodologies, based on the monotonic tension test properties of the wire and from the coefficients obtained from the axial fatigue tests reported by Beretta. In all cases the FE wear simulation has been carried out for 50000 cycles, so in the cases where not crack appears the maximum accumulated damage value and the location of this damage has been listed. The crack location value has been considered as the distance from the centre of the wear scar to the predicted crack position. On the other hand, the experimental tests have been carried out till 200000 number of cycles, so conditions in which cracks could nucleate at longer number of cycles has not been predicted.

The Manson's Universal slopes method predict correctly the lives in the 130 μm cases; nevertheless under predict cracks in the case of 2N-65 μm . The Modified Muralidharan's universal slopes method is more conservative than the previous method, mainly with higher loads such as 4N-65 μm , where the life decrease drastically. Nevertheless the predicted crack location is closest to that one obtained experimentally. The Medians method, which is the last method used to obtain the fatigue coefficients of the thin steel wire analysed in this study is the less conservative method. In the case of 2N-130 μm no crack is predicted. Moreover the crack location position is over predicted. On the other hand the fatigue coefficients obtained from the fatigue tests reported by Beretta, looks to be the most conservative, under predicting cracks in all cases. Nevertheless the predicted crack position is the closest to the one obtained experimentally.

In all cases it is clear that the increase of the load reduce drastically the life of the wire, nevertheless, it is not clear that an increase of the stroke also reduce drastically the life of the wire as shown in the experimental results reported in this study and in the conclusions reported

by Wang et al. [11] where this effect was associated with an increase of the tangential force. Taking into account this last statement, the values predicted with the proposed methodology for 2N-65 μm and 2N-130 μm are similar, so there are more aspects that have to be analysed in order to improve this methodology. These aspects will be summarized in the next section.

Test conditions	Experimental N_f	Predicted N_f			
		Universal Slopes	Modified universal slopes	Medians (steels)	Beretta
90°-4N-65 μm (Crack) ($x=20\text{-}50\ \mu\text{m}$)	$2 \times 10^4\text{-}1 \times 10^5$	5.5×10^3 ($x=92.9\ \mu\text{m}$)	200 ($x=0\ \mu\text{m}$)	1.35×10^4 ($x=92.9\ \mu\text{m}$)	500 ($x=18.31\ \mu\text{m}$)
90°-2N-65 μm (No crack)	$>> 2 \times 10^5$	2.55×10^4 ($x=80.5\ \mu\text{m}$)	7.5×10^3 ($x=80.5\ \mu\text{m}$)	D=0.2042 ($x=80.5\ \mu\text{m}$)	2.5×10^3 ($x=68.13\ \mu\text{m}$)
90°-2N-130 μm (Crack) ($x=80\ \mu\text{m}$)	$1.5 \times 10^4\text{-}5 \times 10^4$	2.45×10^4 ($x=142\ \mu\text{m}$)	1.05×10^4 ($x=117.5\ \mu\text{m}$)	D=0.258 ($x=159.7\ \mu\text{m}$)	3×10^3 ($x=105.2\ \mu\text{m}$)
90°-1N-130 μm (No crack)	$>> 2 \times 10^5$	D=0.313 ($x=142\ \mu\text{m}$)	D=0.314 ($x=142.3\ \mu\text{m}$)	D=0.0208 ($x=142.3\ \mu\text{m}$)	4.5×10^3 ($x=105.2\ \mu\text{m}$)

Table 7. Comparison of measured and predicted lives and failure locations under different SWT coefficients fitting methods (x represents de location from the centre of the wear scar, D represent the damage after 50×10^3 number of cycles).

Fig. 16 shows the damage location plots of the two crack cases presented previously, using the fatigue coefficients obtained from Manson's universal slope method, which is the most consistent with the experimental lives. While Fig. 16a and b show the top view and the axial cut in the transversal maximum damage position (0 ycoord position) for 4N-65 μm and 5500 number of cycles Fig. 16c and d show the plot for 2N-130 μm and 24500 cycles. In both cases it is shown the symmetrical position of the crack location as shown in the experimental tests.

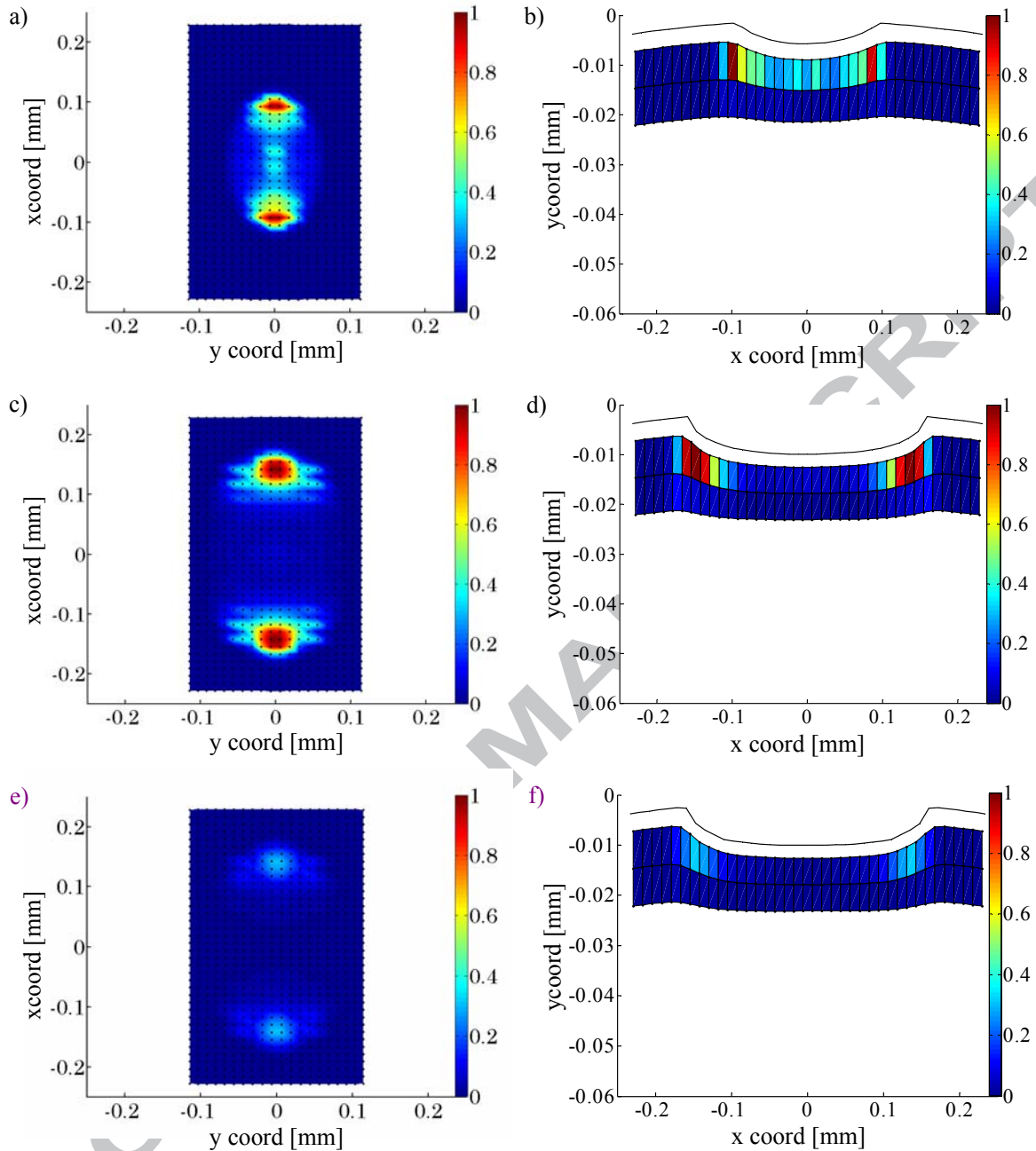


Fig. 16. Predicted location of the failure according to Manson's universal slope coefficients: 4N-65 μm - 5.5×10^3 , a) Top view, b) longitudinal cut; 2N-130 μm - 2.45×10^4 , c) Top view, d) longitudinal cut; 1N-130 μm - 5×10^4 , e) Top view, f) longitudinal cut.

4.4 Fretting wear life prediction methodology discussion

This is the first step to develop a consistent methodology for predicting fretting wear induced cracks in the thin steel wires used in wire rope systems. The presented FE fretting wear simulation model with the combined SWT critical plane and the accumulative damage

methodology, has demonstrated that there are some aspects that have to be improved in order to predict this complex phenomenon in the thin steel wires.

As reported by Meggiolaro and Castro [33], the different methods proposed in this work for obtaining the fatigue coefficients of the wire from the uniaxial monotonic tests, may results in life prediction errors of an order of magnitude, which is in accordance with the values obtained in Table 7 in specific loading cases and methods (over predicting or under predicting cracks). So he proposed these methods as the first stages of design, requiring the experimental fatigue parameters for correct predictions.

On the other hand, when using the fatigue coefficients obtained from the experimental fatigue data reported by Beretta [34] for 1.97 mm wire, the results are over conservative. As shown in the S-N curves reported in the literature [5, 8, 34], different diameters thin steel wires could have different fatigue properties. This is because the fatigue properties of the wires are related to different parameters: such as the interlamellar spacing of the pearlite obtained by the cold-drawn process, the diameter of the wire or the size of the inner defects. The diameter of the wire studied in this work is smaller than those ones reported in the literature. Moreover this wire presents higher ultimate tensile strength and higher yield strength. So future work will be focused in characterize the fatigue behaviour of this wire with the complexity associate to the very small diameter.

The results obtained by the combined FE wear model and SWT critical plane damage methodology, mainly are over conservative. One approach used by many researches to solve this problem is the application of the volume averaging techniques [15-16], such as these methods can capture in more realistic way the stress field corresponding to the crack nucleation. On the other hand, to improve the prediction corresponding to the crack location Ding et al. [36] proposed to combine the Ruiz parameters, which emphasise the importance of the frictional work, with the SWT critical plane approach. When using these types of parameters with volume averaging of the SWT parameter, as the average grain size, Ding et al. [37] reported the effectiveness in the incorporation the wear effects along with the crack nucleation prediction.

Moreover in order to simplify this study a mesh size which is optimum for the wear simulation as described in [21] was used. This mesh size gives good contact results in the great part of the fretting wear test and smaller mesh sizes could increase drastically the computational time. Nevertheless it is known that the stress and strain values are mesh size dependent. Therefore, it is proposed to perform a convergence study with respect to the stress values and the SWT critical plane damage model. Related with this study it has to be taken into account the stress gradients appeared during the fretting problem in the life prediction. It means that volume, line or area averaging techniques have to be taken into account. Around this aspect Sum et al. [17] has previously shown that, in fact, if one averages integration point stresses, or as in this paper uses a centroidal stresses, then the FE essentially provides a volume averaging mechanism,

whereby the element size is the volume or area over which averaging is done. Therefore, it could be more important to carry out an analysis of the life predication for the different loading cases based on the volume of each element, than performing the convergence study with respect to the stress and strain values.

One key factor that has to be considered in this methodology is the introduction a crack propagation model in combination with the developed crack initiation methodology. Such as the methodology proposed by Madge et al. [38] for 2D problems. This approach could explain, that e.g for the 2N-65 μm and 2N-130 μm cases the wear could initiate at the same time, but due to the effect of the wear in the case of 1N-130 μm the crack could propagate and in the case of 2N-65 μm the crack could arrested and disappear.

Future works will be focused in a more exhaustive crack pack identification under different loads and strokes conditions, taking into account also the fretting fatigue tests proposed by Wang et al. [11] for wider diameters, in which more realistic conditions, close to those presented in wire ropes could be tested and used for developing a more robust FE wear crack nucleation and propagation methodology for thin steel wires.

6 Conclusions

This paper has presented a finite element prediction methodology which combines a FE wear model and a critical plane SWT damage accumulation approach for the prediction fretting wear induced cracks in thin steel wires. Four different methods for estimating the fatigue coefficients of the steel wire have been analysed and the fatigue life predictions have been compared to the fretting wear experimental tests carried out on thin steel wires. The main conclusions are:

A significant reduction of the fretting wear frictionally-induced multiaxial contact stresses within the first thousand of cycles is predicted. The maximum tensile stresses are located in the edge of the wear scar in the sliding direction.

The friction coefficient and the bending produced tensile stresses in the wire are two of the parameters that can reduce crack nucleation. Low friction coefficients and low bending pre-stresses are indispensable for increasing the life of the wire.

The high effect presented by the bending induced tensile stresses combined with the fretting multiaxial stresses leads to produce cracks in mode I.

Symmetrical cracks, about the centre of the wear scar, are predicted, as shown experimentally. However, the locations of the cracks obtained experimentally are closer to the centre than the predicted ones.

The lives predicted with this methodology are conservative relative to those obtained experimentally. Manson's method and the median's method gives lives closer to those obtained experimentally, while those predicted with the fatigue

coefficients obtained from the modified universal slopes method and Bereta's fatigue data are the more conservative.

While this approach predicts that increasing load reduces drastically the life of the wire, it does not predict that an increasing stroke also reduces drastically the life of the wire, as shown experimentally.

Finally different solutions for the improvement of this methodology in future works are proposed. These include: the fatigue characterization of the thin steel wires; the introduction of volume-averaging techniques based on the element size or the Ruiz parameters in the SWT critical plane approach to improve the live predictions and the crack locations; development of crack nucleation and propagation methodologies which can explain better the effect of crack propagation or arrest due to the wear and perform fretting-fatigue tests for a more exhaustive crack pack identification which could help in developing a more robust FE wear crack nucleation and propagation methodology for thin steel wires.

Acknowledgments

The authors would like to thank the Basque Government for the financial support under the Universidad Empresa program in the frame of the SIVICA project (Ref. UE2009-5). The authors also would like to thank the reviewers for their helpful comments and discussions.

References

1. K.K. Schrems, Wear related fatigue in a wire rope failure, *J. Test. Eval.* 22 (1994) 490-499.
2. R.B. Waterhouse, Fretting in steel ropes and cable – A review, *ASTM Spec. Tech. Publ.* 1425 (2002) 3-14.
3. M.A. Urchegui, W.Tato, X.Gómez, Wear evolution in a stranded rope subjected to cyclic bending, *J. Mater. Eng. Perform.* 17 (2007) 550-560.
4. J. Llorca, V. Sánchez-Gálvez, Fatigue limit and fatigue life prediction in high strength cold drawn eutectoid steel wires, *Fatigue Fract. Eng. Mater. Struct.* 12 (1985) 31-45.
5. S. Beretta, M. Boniardi, Fatigue strength and surface quality of eutectoid steel wires. *Int. J. Fatigue* 21 (1999) 329-335.
6. J. Petit, C. Sarrazin-Baudoux, F. Lorenzi, Fatigue crack propagation in thin wires of ultra high strength steels, *Procedia Eng.* 2 (2010) 2317-2326.
7. Kasper Lambrighs, Ignace Verpoest, Bert Verlinden, Martine Wevers, Influence of the load ratio on the threshold intensity factor range for heavily drawn steel wires, *Eng. Fail. Anal.* 18 (2011) 694-699.
8. E. Navaei Alvar, J. Aghazadeh Mohandesi, Fatigue damage accumulation in cold-drawn steel wire under variable loading, *Mater. Des.* 31 (2010) 2018-2024.
9. Roberto Brighenti, Andrea Carpinteri, Sabrina Vantadori, Influence of residual stresses on fatigue crack propagation in pearlitic cold-drawn steel wires, *Mater. Sci. Forum* 681 (2011) 229-235.
10. DK. Zhang, SR. Ge, YH. Quiang, Research on the fatigue and fracture behaviour due to the fretting wear of steel wire in hoisting rope, *Wear* 271 (2011) 866-874.
11. DG. Wang, DK. Zhang, SQ. Wang, SR. Ge, Finite element analysis of hoisting rope and fretting wear evolution and fatigue life estimation of steel wires, *Eng. Fail. Anal.* 27 (2013) 173-193.
12. DG. Wang, DK. Zhang, S.R. Ge, Effect of displacement amplitude on fretting fatigue behavior of hoisting rope wires in low cycle fatigue, *Tribol. Int.* 52 (2012) 178-189.
13. DG. Wang, DK. Zhang, SR. Ge, Finite element analysis of fretting fatigue behaviour of steel wires and crack initiation characteristics, *Eng. Fail. Anal.* 28 (2013) 47-62.
14. M.P. Szolwinski, T.N. Farris, Mechanics of fretting fatigue crack formation, *Wear* 198 (1996) 93-107.
15. J. A. Araújo, D. Nowell, The effect of rapidly varying contact stress fields on fretting fatigue, *Int. J. Fatigue* 24 (2002) 763-775.
16. S. Fouvry, P. Duo, Ph. Pruchaut, A quantitative approach of Ti-6Al-4V fretting damage: friction, wear and crack nucleation, *Wear* 257 (2004) 916-929.
17. W. S. Sum, E.J. Williams, S.B. Leen, Finite element, critical-plane, fatigue life prediction of simple and complex contact configurations, *Int. J. Fatigue* 27 (2005) 403-416.
18. J.J. Madge, S.B. Leen, I.R. McColl, P.H. Shipway, Contact-evolution based prediction of fretting fatigue life: Effect of slip amplitude, *Wear* 262 (2007) 1159-1170.
19. T. Zhang, P.E. McHugh, S.B. Leen, Computational study on the effect of contact geometry on fretting behaviour, *Wear* 271 (2011) 1462-1480.
20. A. Cruzado, M. Hartelt, R. Wäsche, M.A. Urchegui, X. Gómez, Fretting wear of thin steel wires. Part 1: influence of contact pressure, *Wear* 268 (2010) 1409-1416.

21. A. Cruzado, M.A. Urchegui, X. Gómez, Finite element modeling and experimental validation of fretting wear scars in thin steel wires, *Wear* 289 (2012) 26-38.
22. I. R. McColl; J. Ding; S. B. Leen, Finite element simulation and experimental validation of Fretting wear, *Wear* 256 (2004) 1114-1127.
23. S. Fouvry, C. Paulin, C. Meunier, Finite element modelling of fretting wear surface evolution: application to a Ti-6Al-4V contact, *Wear* 264 (2008) 26-36.
24. C. Mary, S. Fouvry, Numerical prediction of fretting contact durability using energy wear approach: Optimisation of finite-element model, *Wear* 263 (2007) 444-450.
25. Abaqus User's Manual, Version 6.9, Hibbit, Karlsson & Sorensen, Inc., USA, 2009.
26. C. Navarro, S. Muñoz, J. Domínguez, On the use of multiaxial fatigue criteria for fretting fatigue life assessment, *Int. J. Fatigue* 30 (2008) 32-44.
27. V. Fridrici, S. Fouvry, P. Kapsa, P. Perruchaut, Prediction of cracking in Ti-6Al-4V alloy under fretting-wear: use of the SWT criterion, *Wear* 259 (2005) 300-308.
28. S. Muñoz, H. Proudhon, J. Domínguez, S. Fouvry, Prediction of the crack extension under fretting wear loading conditions, *Int. J. Fatigue* 28 (2006) 1769-1779.
29. J. Das, S.M. Sivakumar. An evaluation of multiaxial fatigue life assesment methods for engineering components, *Int. J. Pres. Ves. Pip.* 76 (1999) 741-746.
30. L. Del Llano-Vizcaya, C. Rubio-González, G. Mesmacque, T. Cervantes-Hernández, Multiaxial fatigue and failure análisis of helical compression Springs, *Eng. Fail. Anal.* 13 (2006) 1303-1313.
31. SS. Manson, Fatigue: a complex subject-some simple approximations, *Exp. Mech.* 5 (1965) 193-226.
32. U. Muralidharan, SS. Manson, Modified universal slopes equation for estimation of fatigue characteristics. *J. Eng. Mater-T. ASME* 110 (1988) 55-58.
33. M.A. Meggiolaro, J. T. P. Castro, Statistical evaluation of strain-life fatigue crack initiation predictions, *Int. J. Fatigue* 26 (2004) 463-476.
34. S. Beretta, S. Matteazzi, Short crack propagation in eutectoid steel wires, *Int. J. Fatigue* 18 (1996) 451-456.
35. I. Verpoest, E. Aernoudt, A. Deruyttere, M. De Bondt, The fatigue threshold, surface condition and fatigue limit of steel wire, *Int. J. Fatigue* 7 (1985) 199-214.
36. J. Ding, W. S. Sum, R. Sabesan, S. B. Leen, I. R. McColl, E. J. Williams, Fretting fatigue predictions in a complex couplings, *Int. J. Fatigue* 29 (2007) 1229-1244.
37. J. Ding, D. Houghton, E. J. Williams, S. B. Leen, Simple parameters to predict effect of surface damage on fretting fatigue, *Int. J. Fatigue* 33 (2011) 332-342.
38. J. J. Madge, S. B. Leen, P. H. Shipway, A combined wear and crack nucleation-propagation methodology for fretting fatigue prediction, *Int. J. Fatigue* 30 (2008) 1509-1528.

Highlights

FE analysis of fretting wear induced multiaxial-stresses in thin steel wires.
Implementation of the SWT critical-plane approach in a 3D FE fretting wear model.
Novel damage accumulation method for 3D FE fretting wear simulation models.
Analysis of different methods for the fatigue coefficients estimation of wires.
Comparison the predicted lives with those obtained in fretting wear tests.

ACCEPTED MANUSCRIPT